**Atmospheric
Chemistry
and Physics**

Quality assessment of O_3 profiles measured by a state-of-the-art ground-based FTIR observing system

M. Schneider[1], F. Hase[1], T. Blumenstock[1], A. Redondas[2], and E. Cuevas[2]

[1]IMK-ASF, Forschungszentrum und Universität Karlsruhe, Karlsruhe, Germany
[2]Centro de Investigación Atmosférico de Izaña, Agencia Estatal de Meteorología, Spain

Abstract. Ground-based Fourier Transform Infra-Red (FTIR) measurements are an important component of the global atmospheric monitoring system. Their essential role in validating satellite measurements requires a precise documentation of their quality. Here we present an extensive quality documentation of ground-based FTIR O_3 profiles. This is done in the form of theoretical and empirical error estimations. The latter is achieved by an intercomparison with ECC-sonde O_3 profiles. The FTIR O_3 amounts are obtained by applying the most advanced instrumentation and retrieval strategies and consequently represent the current potential of this remote sensing technique.

1 Introduction

Ground-based measurements of highly-resolved infrared solar absorption spectra allow ongoing detection of the composition of the atmosphere in a cost-effective manner. They are essential for long-term monitoring and for validating satellite measurements and, thus, they are a vital component of the global atmospheric monitoring system. However, their application as a reference measurement requires precise documentation of their quality. This is often done exclusively by theoretical studies. The errors are then calculated by a method suggested by C. D. Rodgers (Rodgers, 2000). These calculations give a good overview of the achievable data quality, however, they depend on the assumed error sources. Therefore, every assessment of data quality should be completed by a comparison to independent measurements of similar or better quality. Ozone is well suited for such an empiri-

cal quality assessment. It is an important atmospheric constituent and has been monitored over many years by a variety of measurement techniques. In this work we use ECC-sondes (Electro Chemical Cell sondes), launched weekly very close to the FTIR measurement site, for an empirical validation of the FTIR O_3 profiles. The FTIR O_3 profiles are obtained by a optimised retrieval approach (Schneider and Hase, 2008a). While the total column amounts obtained from this approach have already been validated in great detail by an intercomparison to Brewer measurements (Schneider et al., 2008b), in this work we concentrate on the profiles.

Similar validation studies of ground-based FTIR O_3 profiles have already been performed by different authors (Pougatchev et al., 1996; Nakajima et al., 1997; Barret et al., 2002; Schneider et al., 2005a; Kagawa et al., 2007). In some of these works the empirical validation is performed for a very reduced number of sonde-FTIR coincidences, which are furthermore measured within a short time range during specific campaigns. Consequently they poorly represent the actual atmospheric variability. In this work we present an extensive empirical validation consisting of 53 coincident operational ECC sonde and FTIR measurements performed between January 2005 and December 2006 on Tenerife Island. Furthermore, we apply state-of-the-art retrieval strategies and instrumentation. The quality of the FTIR O_3 profiles applied in this paper reflects the current potential of ground-based FTIR systems in monitoring the vertical distribution of atmospheric trace gases which possess weak, strong, isolated and overlapping absorption features (e.g. N_2O, CH_4, H_2O).

In the following section we briefly describe the FTIR instrumentation and retrieval strategy. In Sect. 3 we present the results of our theoretical error estimation. In Sect. 4 we compare the ECC and FTIR O_3 profiles.
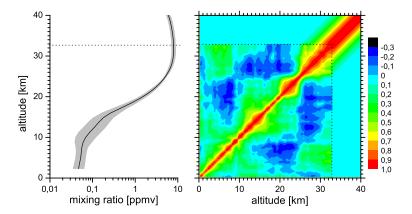
Fig. 1. Left panel: Black line: a priori mean O$_3$ profile and its 1σ variability (shaded area around line) for Tenerife. Right panel: a priori correlation matrix of ozone mixing ratios. Up to 32.8 km, profiles and interlevel correlations are from sonde data measured between 1996 and 2006. Above 32.8 km the values are estimated.

2 FTIR measurements and retrieval strategies

The FTIR measurements were performed at the Izaña Observatory, which is located on the Canary Island of Tenerife, 300 km from the African west coast at 28°18′ N, 16°29′ W at 2370 m a.s.l. From January 1999 to April 2005 a Bruker IFS 120M spectrometer was operated at the site (Schneider et al., 2005b). Since January 2005 we have operated a Bruker IFS 125HR spectrometer. In this work we only evaluate spectra measured by this new IFS 125HR, which offers better performance than the IFS 120M. We use the retrieval code PROFFIT 9.4 (Hase et al., 2004) with the option to retrieve isotopologue ratio profiles (Schneider et al., 2006b). It applies the Karlsruhe Optimised and Precise Radiative Transfer Algorithm (KOPRA, Höpfner et al., 1998; Kuntz et al., 1998; Stiller et al., 1998) as the forward model, which was developed for the analysis of MIPAS-Envisat limb sounder spectra. For the atmospheric O$_3$ retrieval we analyse a combination of small and broad spectral windows between 780–1015 cm^{-1}.

The retrieval strategy is essentially the one described in Schneider and Hase (2008a) and consists of a simultaneous retrieval of O$_3$ and temperature profiles. A priori knowledge of O$_3$ (mean profile and covariances) is taken from an ECC sonde climatology calculated from measurements between 1996 and 2006 as depicted in Fig. 1. It is important to mention that we use the same set of a priori data for all retrievals. We do not vary our a priori depending on season, a strategy often applied in other studies (e.g. Barret et al., 2002). This assures that all variability seen in our profile comes from the measurement and can be easily interpreted. The inversion of the O$_3$ profile is performed on a logarithmic scale. The O$_3$ amounts around the tropopause are highly variable. Under these conditions a logarithmic scale inversion is superior to a linear scale inversion (Hase et al., 2004; Schneider et al., 2006a; Deeter et al., 2007). In the troposphere and middle stratosphere, where the variabilities are smaller, normal and

log-normal distributions are very similar (small shape parameter) and the application of a linear or a logarithmic scale does not significantly affect the result. Furthermore, only the inversion on a logarithmic scale allows for a constraint against ratio profiles, i.e. an optimal estimation of isotopologue ratio profiles (Schneider et al., 2006b). As a priori for the typical ozone isotopologue ratio profiles and their covariances we use data reported by Johnson et al. (2000). The applied temperature a priori profile is a combination of the data from the local ptu-sondes (up to 30 km) and data supplied by the automailer system of the Goddard Space Flight Center. The spectroscopic line parameters are taken from the HITRAN 2004 database (Rothman et al., 2005). For H$_2$O we apply the 2006 updates (Gordon et al., 2007).

3 Theoretical quality assessment

When contemplating remotely-sensed vertical distribution profiles it is important to remember the inherent vertical resolution of these data. Figure 2 shows typical averaging kernels for the retrieved ^{48}O$_3$ profiles and demonstrates that the FTIR measurements contain information about the vertical distribution from the surface up to 40 km. The best vertical resolution is achieved between altitudes of 10 and 20 km, where the FWHM (full width half maximum) of the kernels is around 5 km. The trace (sum of diagonal elements) of the averaging kernel matrix is a measure of the degree of freedom in the measurement. It indicates the number of independent layers present in the retrieved profile. Summing up the diagonal elements of the averaging kernel matrix gives a good overview of the layers that are independently presented in the retrieved profile. We identify as an independent layer the altitude ranges where the sum of the corresponding diagonal entries reaches unity. The right panel of Fig. 2 gives an overview of these layers. It plots the altitude ranges for which the sum of the kernel matrix's diagonal elements reaches unity (x-axis)
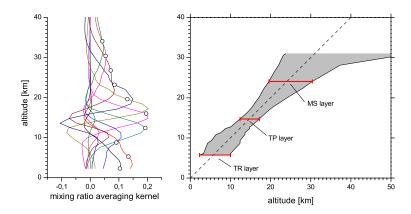
Fig. 2. Left panel: Coloured lines: some typical mixing ratio averaging kernels for the main isotopologue $^{48}O_3$ normalized to 1 km thick layers; open circles: diagonal elements of the kernel matrix. Right panel: altitude ranges for which the sum of the diagonal elements of the kernel matrix reaches 1. The TR, TP, and MS layers are indicated by red bars.

versus the altitude where this layer is centred (y-axis). The centre of the layer is the weighted mean (weighted by kernel matrix's diagonal elements) of the altitudes contributing to the layer. It shows that up to 20 km the FTIR observing system is able to distinguish layers with a vertical extension of smaller than 8 km: e.g. a layer representing the troposphere (surface −10 km, subsequently called the TR layer) or a layer representing the tropopause region (12.5–17 km, TP layer). In the middle stratosphere the vertical resolution is around 10 km (e.g. layer 20–30.5 km, MS layer). The best resolution is achieved at the tropopause, where layers with an extent of 5 km can be distinguished. The uppermost layer that can be resolved extends from 26 km to the top of the atmosphere. Our theoretical error estimation is based on the analytic method suggested by Rodgers (2000), which identifies three error classes: (a) smoothing error, (b) error due to uncertainties in input parameters (instrumental characteristics, spectroscopic data, etc.), and (c) errors due to measurement noise:

$$\hat{x} - x = (\hat{A} - I)(x - x_a)$$
$$+ \hat{G}\hat{K}_p(p - \hat{p})$$
$$+ \hat{G}(y - \hat{y}) \qquad (1)$$

We consider the nonlinearities of the forward model within the variability range of the state vector, therefore, we individually apply Eq. (1) to all members of an ensemble of 500 simulated real states which obeys the a priori statistics: we calculate 500 individual matrices $\hat{A}$ (averaging kernel matrix), $\hat{G}$ (gain matrix), and $\hat{K}_p$ (model parameter sensitivity matrix). In Eq. (1) $\hat{x}$, x, and x_a are the retrieved, real (i.e. $\hat{x} - x$ is the error), and a priori state respectively, $\hat{p}$ and p are the estimated and real model parameters, $\hat{y}$ and y are the measured and simulated spectrum, and I is the identity matrix. This extensive error estimation assures a very accurate error analysis, since it is representative for the whole range of nat-

Table 1. Assumed uncertainties.

error source		random	systematic
phase error		0.01 rad	+0.01 rad
modulation eff.		1%	+1%
z. bl. offset[1]		0.1%	+0.1%
T profile[2]	at surface	1.7 K	−3.5 K
	rest of troposphere	0.7 K	–
	at 30 km	1 K	up to +4 K
	above 50 km	6 K	up to −12 K
solar angle		0.1°	–
line intensity		–	−2%
pres. broad. coef.		–	−5%

[1] zero baseline offset.
[2] for more details please refer to Schneider and Hase (2008a).

urally occurring atmospheric states. Often the errors are only estimated for a typical state, which produces less accurate results since it neglects nonlinearities (matrices $\hat{A}$, $\hat{G}$, and $\hat{K}_p$ depend on the atmospheric state). The assumed error sources are listed in Table 1. These values are critical to the following error estimation. They come from our experiences (e.g. repeatability of ILS (instrumental line shape) measurements) or from references (e.g. the spectroscopic parameter uncertainties are from Rothman et al., 2005). A negative/positive value of an assumed systematic uncertainty means that the in the retrieval a too low/high parameter is used.

Figure 3 shows the standard deviation of the errors calculated for the 500 simulations according to Eq. (1). When considering vertically fine structured profiles, the smoothing error is the leading error since the FTIR system only provides sufficient information about coarse vertical structures. It reaches 25% in the tropopause region, where the actual profile may be highly-structured. The most important
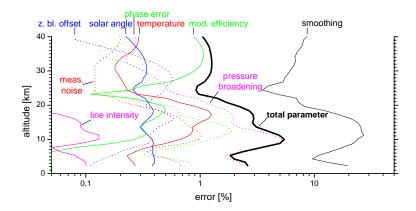
Fig. 3. VMR random errors relative to actual VMRs. Solid black: smoothing; solid green: modulation efficiency; dashed blue: zero baseline offset; solid red: temperature profile; solid blue: solar elevation angle; solid magenta: line intensity; dashed magenta: pressure broadening coefficient; dashed red: measurement noise; thick solid black: total parameter errors (sum of all errors except for smoothing).
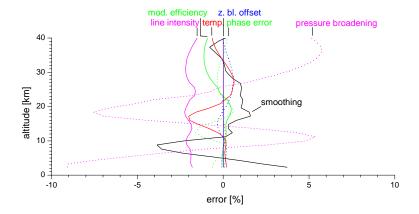

Fig. 4. VMR systematic errors relative to actual VMRs. Line style and colour as in Fig. 3.

Table 2. Estimated random errors relative to climatological amounts (in %) for the 3 layers representing the troposphere, the tropopause region, and the middle stratosphere, and for the layer covering the measurement range of the ECC sonde (surface −30.5 km).

error source	surface −10 km (TR)	12.5–17 km (TP)	20–30.5 km (MS)	surface −30.5 km
smoothing	4.3	13.2	1.3	0.7
phase error	0.2	1.2	0.2	0.2
modulation eff.	< 0.1	0.4	0.3	0.1
zero baseline offset	< 0.1	0.5	0.5	0.3
temperature	< 0.1	1.0	0.2	0.1
solar angle	0.4	0.4	0.3	0.3
line intensity	< 0.1	< 0.1	< 0.1	< 0.1
pres. broad. coef.	1.6	2.4	0.4	0.1
meas. noise	0.3	0.6	0.1	0.1
total	4.0	13.4	1.6	0.8

Table 3. Estimated systematic sensitivity errors and bias errors relative to climatological amounts for the same layers as in Table 2. A dash means that the error is insignificant.

error source	surface −10 km (TR)		12.5–17 km (TP)		20–30.5 km (MS)		surface −30.5 km	
	sensitivity [%]	bias [%]	sensitivity [%]	bias [%]	sensitivity [%]	bias [%]	sensitivity [%]	bias [%]
smoothing	−5.4	+0.5	−10.7	−0.3	−7.2	−0.1	−1.0	−0.3
phase error	−0.1	+0.2	+0.3	+0.7	+0.3	+0.1	+0.2	+0.2
modulation eff.	–	–	+0.2	–	+0.6	+0.3	+0.1	+0.1
zero baseline offset	−0.2	–	−0.3	–	−1.0	−0.5	−0.8	−0.3
temperature	+0.1	–	+1.0	+1.4	−1.2	−0.7	−0.2	−0.3
line intensity	+2.1	+2.0	+1.9	+2.0	+1.9	+1.9	+2.0	+2.0
pres. broad. coef.	+4.7	+4.3	−0.8	+2.3	−2.0	+0.8	–	+1.6
meas. noise	−0.1	–	–	–	+0.1	–	–	–

parameter errors are remaining ILS distortions (instrumental line shape distortions: uncertainties in modulation efficiency and phase error), uncertainties in the temperature profile, and errors in the applied pressure broadening parameter. Even though a systematic error source, the pressure broadening coefficient produces random errors since $\hat{\mathbf{G}}$ and $\hat{\mathbf{K}}_\mathbf{p}$ of Eq. (1) depend on the actual atmospheric state. Figure 4 depicts the systematic errors of the retrieved profiles (mean value of the errors calculated from the 500 simulations). We find that the uncertainty in the pressure broadening coefficient is the most important systematic error source.

If we only consider coarse vertical structures (layers with thickness of 5–10 km) the smoothing error becomes less important. The right panel of Fig. 2 gives a reasonable estimate of the extent of these layers. In Tables 2 and 3 we present the error estimations for the TR, TP, MS layers, and the layer ranging from the surface to 30.5 km. The latter corresponds to the altitudes covered by nearly all ECC sondes. The partial column amount errors of these layers are investigated in great detail. While for the VMR profile errors (Figs. 3 and 4) we restrict the discussion to an estimation of the mean and standard deviation, we analyse the partial column amount errors in more detail. Therefore, we separate them in random error, systematic sensitivity error, and systematic bias error components. Figure 5 illustrates how these different error components are obtained. It depicts the dependence of the error on the actual O$_3$ amount of the MS layer taking the smoothing error as example. The slope of the linear regression line gives the systematic sensitivity error (in our example −7.2%), the offset at the climatological value gives the systematic bias error (−0.2 DU or −0.1% if referred to the climatological amount of the MS layer), and the scattering around the regression line indicates the random error (2.0 DU or 1.3%). This error treatment is described in Schneider and Hase (2008a), which should be consulted for more details.
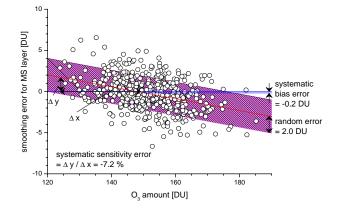

Fig. 5. Dependence of the smoothing error in the MS layer on the actual O$_3$ amount. Separation into error components (random, systematic sensitivity, and systematic bias error) is done by a linear least squares fit. Circles: individual error simulations; red line: linear regression line. Random error: 1σ scattering around the regression line (indicated by magenta area); systematic sensitivity error: slope of the regression line; systematic bias error: offset of the regression line at the a priori value.

For the layers depicted in the right panel of Fig. 2 the sensitivity error does not significantly exceed −10% (i.e. the FTIR system has a sensitivity of around 90%). This is a very satisfactory value, and demonstrates that the high quality measurements together with an advanced retrieval strategy allow an adequate monitoring of these coarse atmospheric structures. An artificial increase of this sensitivity by applying seasonally dependent a priori data is not necessary and would only confuse the interpretation of the FTIR data. Table 3 as well as Fig. 4 show that the systematic errors are dominated by the smoothing error and uncertainties in the spectroscopic line parameters.
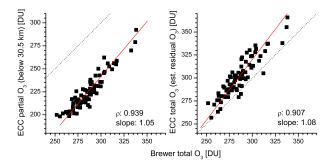
Fig. 6. Comparison between ECC and Brewer O$_3$ amounts. Solid squares: individual coincidences; red lines: regression lines of linear least squares fits; dotted line: diagonal. Left panel: Ignoring the ECC O$_3$ residual. Right panel: considering the ECC O$_3$ residual by assuming a constant mixing ratio from the balloon's burst altitude to the top of the atmosphere.

4 Empirical quality assessment

For this assessment we compare the FTIR O$_3$ (sum of ^{48}O$_3$, ^{50}O$_3$, and ^{49}O$_3$ isotopologues) profiles with regularly performed ECC-sonde measurements. The ozone sonde program on Tenerife started in November 1992 using ECC-sondes (type: Scientific Pump 6A). The sondes are launched weekly from Santa Cruz de Tenerife (35 km northeast of the Observatory) and since October 2006 from Güimar (15 km south of the Observatory). In March 2001 Izaña's ECC-sonde together with the Brewer, DOAS, and FTIR activities were accepted by the NDACC (Network for Detection of Atmospheric Composition Change, http://www.ndacc.org/, formerly called NDSC: Network for Detection of Stratospheric Change, Kurylo, 1991, 2000) as a complementary observing site.

The ECC-sondes generally burst between 30 and 34 km. To use as many sondes as possible and to homogenize the study we use only ECC data measured up to 30.5 km. This altitude is reached by around 90% of all sondes. These criteria provide 53 coincident ECC and FTIR measurements (for 33 different ECC measurements).

4.1 Quality check for ECC-sondes

Schneider et al. (2008b) demonstrates the high quality of the FTIR total column amounts by an extensive intercomparison to Brewer data. A correlation coefficient of 0.992 and an agreement within 0.6% between coincident measurements of O$_3$ total column amounts allowed to conclude that both techniques have a precision of better than 0.5%.

Here we make an analogous brief study for the ECC amounts. As aforementioned we only apply ECC data for altitudes below 30.5 km. However the residual O$_3$ partial column above this altitude is still around 20% of the total O$_3$ amount. From the HALOE climatology (Grooß and Rus-

sell III, 2005) we deduce a 1σ value for the O$_3$ variability above 30.5 km of typically 10–15%. Assuming a vertical correlation length of 2.5 km (which corresponds to the length derived from the ECC data around 30 km), we estimate a 1σ variability for the O$_3$ residual of 4 DU. The left panel of Fig. 6 shows the correlation between Brewer total O$_3$ amounts and ECC partial O$_3$ amounts below 30.5 km for all 80 Brewer/ECC coincidences during 2005 and 2006. We calculate a difference of 60.6$\pm$6.8 DU. Approximately 4 DU of the scatter between the Brewer and ECC data is caused by ignoring the ECC O$_3$ residual. Since the Brewer total column amounts are very precise (around 1.5 DU), there is a remaining scatter of around $\sqrt{6.8^2 - 4^2 - 1.5^2} \approx 5.3$ DU (or around 2.0% if referred to the typical amount), which can be attributed to errors in the ECC data or to the observation of different airmasses by the Brewer, on the one hand, and by the ECC sonde, on the other hand. However, this 2.0% is already less than estimated by the laboratory study of Smit and Sträter (2004), which determines an uncertainty of 6% for the Scientific Pump 6A ECC-sonde type. Furthermore, we found no single outlier for all sondes from 2005 and 2006. Consequently we can conclude that the Izaña ECC sonde measurements are of very high quality.

As is common practice among NDACC sonde users the O$_3$ residual is estimated by extending the mixing ratio measured at the balloon's burst altitude up to the top of the atmosphere. The right panel of Fig. 6 depicts the Brewer total O$_3$ versus the ECC total O$_3$ calculated for the so-estimated O$_3$ residual. Naturally the difference to the Brewer amounts is now smaller (compare right to the left panel). However, we observe a slightly poorer correlation, i.e. more scatter between both experiments. This indicates that, at least at the subtropical site of Izaña, extending the mixing ratio value measured at the sonde's burst altitude until the top of the atmosphere is not suited to estimate the real variability of the O$_3$ residual.

4.2 FTIR versus ECC-sonde

When validating remotely-sensed vertical distribution profiles it is important to remember the inherent vertical resolution of these data. There are two possibilities to adequately validate remotely-sensed profiles: (a) degrade the vertical resolution of the vertically highly-resolved data towards the vertically poorly-resolved data. By this means we exclude the smoothing error from the comparison. In our case the ECC in-situ measurements are vertically highly resolved. (b) Another possibility is to compare only the rough structures that are supposed to be resolvable by the remote sensing measurements. We estimated these structures in Sect. 3 and depict them in the right panel of Fig. 2. In the following we compare FTIR and ECC profiles applying both method (a) and method (b).

4.2.1 Comparison of FTIR and smoothed ECC profiles

The smoothing (or degradation) of the vertically highly-resolved ECC profile $\boldsymbol{x}_{\mathrm{ECC}}$ is done by convolving it with the FTIR averaging kernels $\hat{\mathbf{A}}$:

$$\hat{\boldsymbol{x}}_{\mathrm{ECC}} = \hat{\mathbf{A}}(\boldsymbol{x}_{\mathrm{ECC}} - \boldsymbol{x}_a) + \boldsymbol{x}_a \qquad (2)$$

The result is an ECC profile ($\hat{\boldsymbol{x}}_{\mathrm{ECC}}$) with the same smoothing error as the FTIR profile. Consequently the difference between FTIR and smoothed ECC profile eliminates the smoothing error component, which is the leading error component. Equation (2) requires ECC profile data beyond 30.5 km. However, this data is not available and we extend the ECC profile with the zonally averaged HALOE climatological profile used as a priori in the FTIR retrieval. Consequently the smoothed ECC profile is a combination of two experiments: the ECC and HALOE experiments. The climatological HALOE data neglect the actual variabilities above 30.5 km, which introduces additional random errors above and below 0.5 km. Figure 7 depicts the mean and standard deviation for the difference between FTIR and smoothed ECC profile. These calculations are comparable to the error estimations presented in Figs. 3 and 4. The grey shaded area indicates the total random error of the FTIR profiles (excluding the smoothing error, thick black line in Fig. 3). The light grey shaded area indicates the sum of the FTIR and ECC random errors, i.e. the expected scatter between both experiments. For the ECC random error we assumed 6% as suggested in Smit and Sträter (2004). From the surface up to 27 km we observe a slight altitude dependent but not significant systematic difference. It is +2% at the surface and at 27 km and −10% at 12 km. These differences are probably due to incorrect line parameterisations (error in the pressure broadening coefficient (compare to Fig. 3). Above 28 km we observe a significant systematic difference of up to 16%. Since we compare a combination of ECC sonde and HALOE with FTIR it is difficult to interpret this observation. The reason may be a systematic underestimation of the ECC sondes above 25 km, systematic FTIR errors (due to line parameterisation), or systematic differences between the applied HALOE climatology and the actual climatology above Tenerife.

The observed scatter between FTIR and ECC is a mean of 5% (between the surface and 30.5 km). It is highest between 10 and 15 km where it reaches 10%. It is in satisfactory agreement with the expected errors of around 7% (light grey shaded area of Fig. 7). The slightly higher scatter may be due to the observation of different airmasses by FTIR and ECC or due to a weak overestimation of the theoretical vertical resolution of the FTIR. It is important to mention that Fig. 7 provides no comprehensive documentation of the quality of the FTIR profile. This is only possible together with the averaging kernels: Schneider et al. (2005a) also reports an agreement within 5–10% to ECC sondes but for FTIR profiles obtained from spectra of poorer quality and
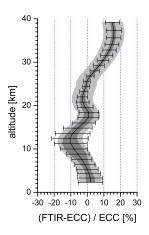

Fig. 7. Difference between FTIR and smoothed ECC sonde profiles. Shown are mean and standard deviation of the difference for the 53 FTIR/ECC coincidences. The grey shaded area indicates the expected FTIR error (excluding the smoothing error); the light grey shaded area indicates the expected random error of (FTIR-ECC)/ECC.

non-optimised retrieval strategies. This leads to broader averaging kernels and provides a stronger smoothing of the ECC profile. The agreement is similar, but the compared vertical structures are much coarser.

4.2.2 Comparison of partial column amounts

A straight forward comparison of partial columns has the advantage that the results are easy to interpret. Figure 8 depicts the correlation of the TR, TP, MS and surface −30.5 km partial columns calculated from the FTIR and original (not smoothed) ECC sonde data. We observe a very good agreement between the FTIR and ECC partial column amounts. For the TR and TP layers we get correlation coefficients of at least 0.96. For the MS layer we still get a coefficient of 0.92 and for the layer from the surface up to 30.5 km a coefficient of 0.96. The scattering around the regression line is 1.5 DU (or 6.8% if related to the climatological amounts) for the TR layer, 1.6 DU (12.1%) for the TP layer, 3.0 DU (1.8%) for the MS layer, and 5.2 DU (2.4%) for the layer from the surface to 30.5 km. This observed scatter agrees very well with the estimated FTIR random errors of Table 2.

Concerning the systematic differences we expect a sensitivity error for the FTIR data of −5.4% and −7.2% for the TR and MS layer, respectively, and a larger error of around −11% for the TP layer (see Table 3), which is confirmed by the FTIR/ECC intercomparison. Figure 8 shows higher slopes for the TR and MS layers (0.95 and 0.87, respectively) than for the TP layer (0.83). The observed systematic bias, if related to the climatological amounts, is $\frac{-0.61\,\mathrm{DU}}{21.97\,\mathrm{DU}} = -2.8\%$ for the TR layer, $\frac{0.64\,\mathrm{DU}}{12.55\,\mathrm{DU}} = +5.1\%$ for the TP layer, and $\frac{3.73\,\mathrm{DU}}{160.75\,\mathrm{DU}} = +2.3\%$ for the MS layer, respectively. For the
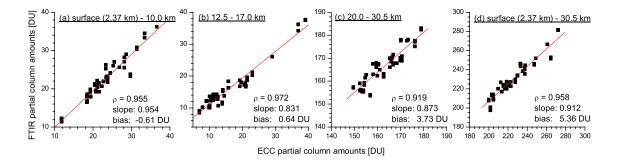
Fig. 8. Correlation between FTIR and ECC measurements. Black squares: individual measurements; red lines: linear regression line of least squares fits. **(a)** TR layer, **(b)** TP layer, **(c)** MS layer, **(d)** layer from surface −30.5 km.

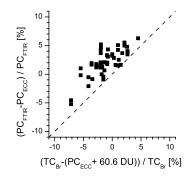**Fig. 9.** Correlation between differences Brewer-ECC and differences FTIR-ECC.

layer between the surface and 30.5 km it is $\frac{5.36\,\mathrm{DU}}{218.62\,\mathrm{DU}}$=+2.5%. These values are all in good agreement to the estimations of Table 3.

In Sect. 4.1 we compared the Brewer total O$_3$ amounts to the ECC O$_3$ amounts between the surface and 30.5 km. This comparison reveals a remaining scatter of around 2%, which can be contributed to errors in the ECC measurements or to the observation of different airmasses by the two experiments. Brewer and FTIR observe the same airmass (they have the same observation geometry) and the disagreement between Brewer and ECC, on the one hand, and between FTIR and ECC, on the other hand, are in deed very similar. This is demonstrated in Fig. 9, which shows the differences between the ECC partial column amounts (PC$_{\mathrm{ECC}}$=$\int_{2.37\,\mathrm{km}}^{30.5\,\mathrm{km}} x_{\mathrm{ECC}}(z)dz$) and the Brewer total column amounts (TC$_{\mathrm{Brewer}}$) versus the differences between the ECC and FTIR partial column amounts (PC$_{\mathrm{FTIR}}$=$\int_{2.37\,\mathrm{km}}^{30.5\,\mathrm{km}} x_{\mathrm{FTIR}}(z)dz$). We can use the Brewer data to account for the observation of different airmasses or for the errors in the ECC data. Therefore we nor-

malise the ECC data to the Brewer total column amounts:

$$x_{\mathrm{ECC,norm}} = \frac{\mathrm{TC}_{\mathrm{Brewer}}}{\mathrm{PC}_{\mathrm{ECC}} + 60.6\,\mathrm{DU}} x_{\mathrm{ECC}} \qquad (3)$$

Here 60.6 DU is the mean value of the residual O$_3$ amount. Figure 10 compares the normalised ECC partial column amounts to the FTIR partial column amounts. This Figure gives a good insight into the real performance of the FTIR system. The normalisation according to Eq. (3) produces changes of about 5% if referred to the typical O$_3$ amounts (see Fig. 9). In the stratosphere the natural variability is of a similar magnitude (5–10%), and the normalisation to the Brewer data significantly improves the correlation between FTIR and ECC partial columns (compare panel (c) of Fig. 10 and 8). On the other hand, in the troposphere or tropopause region the natural variability is very large (between 30% and 70%) and an alteration of the ECC data by only 5% has no significant effect

At Izaña the simultaneously performed high quality total column amount measurements can be used to check the ECC data quality. In Sect. 4.1 we checked the ECC data quality by a comparison to Brewer total column amounts. The confidence of this quality check is limited by the observation of different airmasses, by the variability of the residual O$_3$ above the sonde's burst altitude, and by errors of the measured total column amounts. Already the ignorance of the residual O$_3$ variability (which is about 4 DU or 1.4%) and the error of the Brewer data (about 0.5%) limit the validity of this test to $\sqrt{1.4^2+0.5^2}$=1.5%. This uncertainty range becomes even larger if the balloon bursts below 30.5 km. As demonstrated in this paper a state-of-the-art FTIR system provides partial column amounts of good quality. At super sites like Izaña the quality of the ECC sondes can be checked by the FTIR partial column amounts. This enables good quality checks even for sondes whose balloon's burst at lower altitudes. For sondes reaching 30.5 km the quality check can be performed with a precision of 0.8% (0.8% is the estimated random error for the FTIR partial column amounts below 30.5 km; see Table 2).
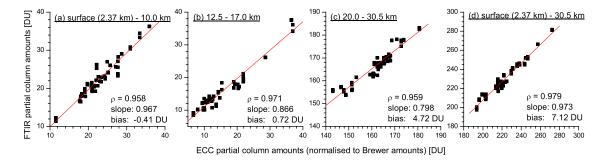
Fig. 10. Same as Fig. 8 but for ECC data normalized to Brewer total column amounts.

5 Summary and conclusions

We have made an extensive theoretical error estimation for O_3 profiles measured by a carefully characterised (regular ILS calibrations) state-of-the-art ground-based FTIR observing system. The FTIR system provides high quality data with a vertical resolution of 4.5–7 km for O_3 amounts below 20 km and of around 10 km in the middle stratosphere. The altitude range with the best vertical resolution coincides with the tropopause region. The application of a unique a priori facilitates the interpretation of annual cycles. We do not recommend the usage of seasonally varying a priori data since this may introduce artificial variabilities and thus strongly reduce the validity of the FTIR data. Our study clearly shows that the FTIR measurement alone contains sufficient information to detect the atmospheric variabilities. This is also true for the high variability in case of lower/middle stratospheric polar O_3 destruction (Kopp et al., 2003).

At the Izaña Observatory ECC sonde, Brewer, and FTIR measurements are performed continuously at high quality. This offers unique conditions for intercomparing these different O_3 monitoring techniques, and an opportunity to document their quality. Such quality checks are essential if the measurements are to be applied for the validation of satellites. The comparison between ECC and FTIR amounts agrees with our theoretical estimations concerning the FTIR precision. Furthermore, it indicates that the ECC sonde provides data with a precision of better than 5% from the surface up to the middle stratosphere. This demonstrated good performance of the ECC measurements is an in-field confirmation of extensive laboratory studies (Smit and Sträter, 2004). We found that the FTIR O_3 partial column amounts between the surface and 30.5 km are typically larger than the corresponding ECC amounts ($\frac{(PC_{FTIR}-PC_{ECC})}{PC_{ECC}}=(2.3\pm2.4)\%$). This result complements the observation of Schneider et al. (2008b) of a systematic difference of $(4\pm1)\%$ between Izaña's FTIR and Brewer total O_3 amounts.

We chose O_3 as the object of our assessment of ground-based FTIR profile measurements because O_3 offers a unique opportunity of comparison to other measurement techniques. The good confirmation of our theoretical error estimation by the empirical comparisons strengthens the validity of future FTIR profile error estimations of other absorbers like N_2O, HF, HCl, CO_2, etc., which, due to the absence of other co-located measurement techniques, are difficult to be confirmed empirically.

References

Barret, B., De Mazière, M., and Demoulin, P.: Retrieval and characterization of ozone profiles from solar infrared spectra at the Jungfraujoch, J. Geophys. Res, 107, 4788–4803, 2002.

Deeter, M. N., Edwards, D. P., and Gille, J. C.: Retrievals of carbon monoxide profiles from MOPITT observations using lognormal a priori statistics, J. Geophys. Res., 112, D11311, doi:10.1029/2006JD007999, 2007.

Gordon, E. I., Rothman, L. S., Gamache, R. R., Jacquemart, D., Boone, C., Bernath, P. F., Shephard, M. W., Delamere, J. S., and Clough, S. A.: Current updates of the water-vapor line list in HITRAN: A new "Diet" for air-broadened half-widths, J. Quant. Spectrosc. Radiat. Transfer, 108, 389–402, 2007.

Grooß, J.-U. and Russell III, J. M.: Technical note: A stratospheric climatology for O_3, H_2O, CH_4, NO_x, HCl, and HF derived from HALOE measurements, Atmos. Chem. Phys., 5, 2797–2807, 2005,
http://www.atmos-chem-phys.net/5/2797/2005/.

Hase, F., Hannigan, J. W., Coffey, M. T., Goldman, A., Höpfner, M., Jones, N. B., Rinsland, C. P., and Wood, S. W.: Intercomparison of retrieval codes used for the analysis of high-resolution, ground-based FTIR measurements, J. Quant. Spectrosc. Radiat. Transfer, 87, 25–52, 2004.

Höpfner, M., Stiller, G. P., Kuntz, M., von Clarmann, T., Echle, G., Funke, B., Glatthor, N., Hase, F., Kemnitzer, H., and Zorn, S.: The Karlsruhe optimized and precise radiative transfer algorithm, Part II: Interface to retrieval applications, SPIE Proceedings 1998, 3501, 186–195, 1998.

Johnson, D. G., Jucks, K. W., Traub, W. A., and Chance, K. V.: Isotopic composition of stratospheric ozone, J. Geophys. Res., 105, 9025–9031, 2000.

Kagawa, A., Kasai, Y., Jones, N. B., Yamamori, M., Seki, K., Murcray, F., Murayama, Y., Mizutani, K., and Itabe, T.: Characteristics and error estimations of stratospheric ozone and ozone-related species over Poker Flat (65° N, 147° W), Alaska observed by a ground-based FTIR spectrometer from 2001 to 2003, Atmos. Chem. Phys., 7, 3791–3810, 2007,
http://www.atmos-chem-phys.net/7/3791/2007/.

Kopp, G., Berg, H., Blumenstock, T., Fischer, H., Hase, F., Hochschild, G., Hpfner, M., Kouker, W., Reddmann, T., Ruhnke, R., Raffalski, U., and Kondo, Y.: Evolution of ozone and ozone related species over Kiruna during the THESEO 2000-SOLVE campaign retrieved from ground-based millimeter wave and infrared observations, J. Geophys. Res., 108, 8308, 2003.

Kuntz, M., Höpfner, M., Stiller, G. P., Clarmann, T. v., Echle, G., Funke, B., Glatthor, N., Hase, F., Kemnitzer, H., and Zorn, S.: The Karlsruhe optimized and precise radiative transfer algorithm, Part III: ADDLIN and TRANSF algorithms for modeling spectral transmittance and radiance, SPIE Proceedings 1998, 3501, 247–256, 1998.

Kurylo, M. J.: Network for the detection of stratospheric change (NDSC), SPIE Proceedings 1991, Remote Sensing of Atmospheric Chemistry, 1491, 168–174, 1991.

Kurylo, M. J. and Zander, R.: The NDSC – Its status after 10 years of operation, Proceedings of XIX Quadrennial Ozone Symposium, Hokkaido University, Sapporo, Japan, 167–168, 2000.

Nakajima, H., Liu, X., Murata, I., Kondo, Y., Murcray, F. J., Koike, M., Zhao, Y., and Nakane H.: Retrieval of vertical profiles of ozone from high-resolution infrared solar spectra at Rikubetsu, Japan, J. Geophys. Res., 102, 29 981–29 990, 1997.

Pougatchev, N. S., Connor, B. J., Jones, N. B., and Rinsland, C. P.: Validation of ozone profile retrievals from infrared ground-based solar spectra, Geophys. Res. Lett., 23, 1637–1640, 1996.

Rodgers, C. D.: Inverse Methods for Atmospheric Sounding: Theory and Praxis, World Scientific Publishing Co., Singapore, ISBN 981-02-2740-X, 2000.

Rothman, L. S., Jacquemart, D., Barbe, A., Benner, D. C., Birk, M., Brown, L. R., Carleer, M. R., Chackerian Jr., C., Chance, K. V., Coudert, L. H., Dana, V., Devi, J., Flaud, J.-M., Gamache, R. R., Goldman, A., Hartmann, J.-M., Jucks, K. W., Maki, A. G., Mandin, J.-Y., Massie, S. T., Orphal, J., Perrin, A., Rinsland, C. P., Smith, M. A. H., Tennyson, J., Tolchenov, R. N., Toth, R. A., Vander Auwera, J., Varanasi, P., and Wagner, G.: The HITRAN 2004 molecular spectroscopic database, J. Quant. Spectrosc. Radiat. Transfer, 96, 139–204, 2005.

Schneider M., Blumenstock, T., Hase, F., Höpfner, M., Cuevas, E., Redondas, A., and Sancho, J. M.: Ozone profiles and total column amounts derived at Izaña, Tenerife Island, from FTIR solar absorption spectra, and its validation by an intercomparison to ECC-sonde and Brewer spectrometer measurements, J. Quant. Spectrosc. Radiat. Transfer, 91, 245–274, 2005a.

Schneider, M., Blumenstock, T., Chipperfield, M. P., Hase, F., Kouker, W., Reddmann, T., Ruhnke, R., Cuevas, E., and Fischer, H.: Subtropical trace gas profiles determined by ground-based FTIR spectroscopy at Izaa (28° N, 16° W): Five-year record, error analysis, and comparison with 3-D CTMs, Atmos. Chem. Phys., 5, 153–167, 2005b,
http://www.atmos-chem-phys.net/5/153/2005/.

Schneider, M., Hase, F., and Blumenstock, T.: Water vapour profiles by ground-based FTIR spectroscopy: study for an optimised retrieval and its validation, Atmos. Chem. Phys., 6, 811–830, 2006a,
http://www.atmos-chem-phys.net/6/811/2006/.

Schneider, M., Hase, F., Blumenstock, T.: Ground-based remote sensing of HDO/H$_2$O ratio profiles: introduction and validation of an innovative retrieval approach, Atmos. Chem. Phys., 6, 4705–4722, 2006b,
http://www.atmos-chem-phys.net/6/4705/2006/.

Schneider, M. and Hase, F.: Technical note: Recipe for monitoring of total ozone with a precision of 1 DU applying mid-infrared solar absorption spectra, Atmos. Chem. Phys., 8, 63–71, 2008a,
http://www.atmos-chem-phys.net/8/63/2008/.

Schneider, M., Redondas, A., Hase, F., Guirado, C., Blumenstock, T., and Cuevas, E.: Comparison of ground-based Brewer and FTIR total column O$_3$ monitoring techniques, Atmos. Chem. Phys., 8, 5535–5550, 2008b,
http://www.atmos-chem-phys.net/8/5535/2008/.

Smit, H. G. J. and Sträter, W.: JOSIE-2000: Jülich Ozone Sonde Intercomparison Experiment 2000, World Meteorological Organization, Global Atmosphere Watch, Report No. 158, 2004.

Stiller, G. P., Höpfner, M., Kuntz, M., Clarmann, T. v., Echle, G., Fischer, H., Funke, B., Glatthor, N., Hase, F., Kemnitzer, H., and Zorn, S.: The Karlsruhe optimized and precise radiative transfer algorithm, Part I: Requirements, justification and model error estimation, SPIE Proceedings 1998, 3501, 257–268, 1998.